# Impact of two geostatistical hydro-facies simulation strategies on head statistics under non-uniform groundwater flow

Raul Perulero Serrano [a], Laura Guadagnini [a], Monica Riva [a,b,*], Mauro Giudici [c,d,e], Alberto Guadagnini [a,b]

[a] Politecnico di Milano, Dipartimento di Ingegneria Civile e Ambientale (DICA), Piazza L. Da Vinci, 32, 20133 Milano, Italy
[b] University of Arizona, Department of Hydrology and Water Resources, Tucson, AZ 85721, USA
[c] Università degli Studi di Milano, Dipartimento di Scienze della Terra "Ardito Desio", Via Cicognara 7, 20129 Milano, Italy
[d] CNR-IDPA (Consiglio Nazionale delle Ricerche, Istituto per la Dinamica dei Processi Ambientali), via Mario Bianco 9, 20131 Milano, Italy
[e] CINFAI (Consorzio Interuniversitario Nazionale di Fisica delle Atmsofere e delle Idrosfere), c/o, Università degli Studi di Milano, via Cicognara 7, 20129 Milano, Italy

## 1. Introduction

The present work is focused on the assessment of the impact on hydraulic head statistics of two geostatistically-based methodologies for the stochastic simulation of the spatial arrangement of hydro-facies in field scale aquifer systems. The relevance of an appropriate characterization of the probability distribution of hydraulic heads is critical in the context of Probabilistic Risk Assessment (PRA) procedures which are nowadays considered as viable procedures to estimate the risk associated with catastrophic events in environmental problems (Tartakovsky, 2013 and references therein). Application of PRA to actual settings typically requires the estimate of the probability density function (pdf) of a target environmental performance metric (EPM, a terminology introduced by De Barros et al., 2012). In the groundwater literature, the functional format of probability distributions of solute travel/residence times, trajectories and concentrations has been extensively analyzed during the last years (Fiorotto and Caroni, 2002; Bellin and Tonina, 2007; Riva et al., 2008, 2010; Schwede et al., 2008; Enzenhoefer et al., 2012 amongst others). On the other hand, less attention has been devoted to study the probability distribution of hydraulic head, $h$, in complex groundwater systems and under non-uniform (in the mean) flow conditions. These settings are crucial for the analysis of the (negative) consequences arising from events associated with the occurrence of $h$ dropping below or rising above a given threshold. These basic events are critical for various goal oriented risk assessment practices, including, e.g., the

\* Corresponding author. Tel.: +39 02 2399 6214.
   E-mail address: monica.riva@polimi.it (M. Riva).

protection of natural springs or ponds or the prevention of damages to underground infrastructures, and constitute core requirements in the planning of groundwater abstraction procedures or during the design of protection barriers. In this context, estimates of first and second (conditional or unconditional) statistical moments of $h$ have been largely analyzed by means of analytical (e.g., Guadagnini et al., 2003; Riva and Guadagnini, 2009 and references therein) or numerical (e.g., Guadagnini and Neuman, 1999b; Hernandez et al., 2006) methods for bounded randomly heterogeneous aquifers under the action of pumping. Low-order (statistical) moments (i.e., mean and variance–covariance) of hydraulic heads in unbounded and bounded domains under uniform (in the mean flow) conditions have been investigated, amongst others, by Dagan (1985, 1989), Rubin and Dagan (1988, 1989), Ababou et al. (1989), Osnes (1995), Guadagnini and Neuman (1999a,b). Even as these low-order moments have a considerable theoretical and practical interest, they are not directly suitable to PRA protocols where the behavior of the tails of the target variable distribution needs to be identified. This behavior can differ from the one dictated by the classically assumed Gaussian or lognormal distributions and can be influenced by the type of system heterogeneity, hydraulic boundaries and source/sink terms, as we discuss in this work.

Jones (1990) observed the non-Gaussian shape of heads pdf close to pumping wells in a two-dimensional confined aquifer where the transmissivity is lognormally distributed and spatially correlated according to an exponential covariance model. Kunstmann and Kastens (2006) modeled an aquifer in Gambach (Germany) under general non-uniform flow conditions as a two-dimensional, block-heterogeneous system, where transmissivity is homogeneous within each of five considered distinct zones. These authors noted that groundwater velocities could be well approximated by lognormal distributions while heads could be best described by long-tailed pdfs (such as the Weibull or the Gamma distributions). Nowak et al. (2008) presented a detailed numerical study centered on the analysis of statistical moments and pdf of heads and velocity components. Their work involved three-dimensional flow through realizations of randomly heterogeneous conductivity fields subject to uniform mean flow conditions. The authors noted that the shape of heads pdf is similar to a Gaussian or a Beta distribution at locations which were respectively far or close to the Dirichlet boundaries. The longitudinal discharge components appeared to be well interpreted by a lognormal distribution while their transverse counterparts displayed long tails. Additional studies which are concerned with key statistics of groundwater fluxes under uniform (in the mean) flow conditions include the works of Englert et al. (2006) and Zarlenga et al. (2012).

The selection of a model through which one can describe the natural heterogeneity of a system is a key point in the analysis of the distribution of groundwater flow (and possibly transport) variables. The model choice strongly depends on the scale of investigation. At the large field scale, geological heterogeneity of sedimentary bodies can be represented and modeled from information on depositional facies distributions. Statistical grid-based sedimentary facies reconstruction and modeling (FRM) methods can be employed to provide consistent representations of facies distribution and are amenable to include conditioning to hard and/or soft data. Falivene et al. (2007) provide an overview of the most widely used deterministic and stochastic FRM methods, including pixel-based methods termed as Sequential Indicator (SISIM), transition probability schemes (e.g., T-PROGS; Carle, 1999), multiple point simulation (Strebelle, 2002; Zhang et al., 2006; Wu et al., 2008), truncated Gaussian (TGS) and plurigaussian (TPS) simulation.

Sequential Indicator algorithms are widespread geostatistical simulation techniques that rely on indicator (co-)kriging. These have been applied to diverse datasets to study the influence of the random distribution of aquifer sedimentological facies on target environmental variables. In this context, Riva et al. (2006) present a synthetic numerical Monte Carlo study aimed at analyzing the relative importance of uncertain facies architecture and hydraulic attributes (hydraulic conductivity and porosity) on the probabilistic distribution of three-dimensional well catchments and time-related capture zones. The authors base their comparative study on a rich data-base comprising sedimentological and hydrogeological information collected within a shallow alluvial aquifer system. Riva et al. (2008, 2010) adopt the same methodology to interpret the results of a field tracer test performed in the same setting. These authors consider diverse conceptual models to describe the system heterogeneity, including scenarios where the facies distribution is random and modeled through a SISIM-based technique and the hydraulic properties of each material are either random or deterministically prescribed. Comparisons between the ability of diverse geostatistical methods to reproduce key features of field-scale aquifer systems have been published in the literature (e.g., Casar-González, 2001; Falivene et al., 2006; Scheibe and Murray, 1998; Dell'Arciprete et al., 2012). Lee et al. (2007) performed a set of Monte Carlo simulations to mimic a pumping test in an alluvial fan aquifer using the sequential Gaussian simulation method and the transition probability indicator simulation. Emery (2004) highlights limitations of SISIM upon examining the conditions under which a set of realizations is consistent with the input parameters.

Truncated Gaussian simulation enables one to condition simulations on prior information stemming from various sources while guaranteeing consistency between variogram and cross-variogram of the variables considered. The possibility of using a multiplicity of Gaussian functions to codify hydro-facies extends the potential of TGS and is the cornerstone of TPS (Galli et al., 1994). TPS allows taking into account complex transitions between material types and simulating anisotropic distributions of litho-types, whereas TGS explicitly considers only sequentially ranked categories. The application of TPS usually aims at (a) assessing the uncertainty associated with the location of the internal boundaries demarcating geo-materials within the domain, and (b) improving the geological constraints in the characterization of quantitative attributes, such as mineral ore grades. TPS is typically employed to simulate geological domains in diverse contexts, including petroleum reservoirs and mineral deposits, spatial arrangement of hydro-facies in aquifers, or soil types at a catchment scale (e.g., Betzhold and Roth, 2000; Dowd et al., 2007; Mariethoz et al., 2009).

The study of the relative impact of diverse conceptualization and simulation techniques to represent random hydro-facies spatial arrangement on the probabilistic distribution of hydraulic heads in three-dimensional aquifer systems under non-uniform mean flow conditions of the kind that is associated with large scale field settings is still lacking. As highlighted above, this analysis is tied to Probabilistic Risk Assessment procedures and constitutes one of the steps which can be adopted in modern PRA applications based on the idea of decomposing the full problem (that might comprise several uncertainty sources, including those associated with hydro-stratigraphic structure, aquifer recharge, boundary conditions, location and/or pumping/injection rate of wells) into sets of basic events (e.g., Bolster et al., 2009; Jurado et al., 2012; Tartakovsky, 2013 and references therein).

Here, we perform a numerical Monte Carlo study based on a geological system whose heterogeneous structure mimics the one associated with an alluvial aquifer system located in northern Italy where abundant lithological and geological information are available. Our analysis considers a non-uniform flow scenario due to the superimposition of a base uniform (in the mean) flow and the action of a pumping well. Field-scale available lithological

data are analyzed to characterize prevalent litho-type categories and the associated geological contact rules. The simulation domain is modeled as a composite medium with randomly distributed hydro-facies, each associated with a given hydraulic conductivity. Collections of conditional Monte Carlo realizations of the three-dimensional geo-materials distributions are generated by (i) a classical indicator-based approach and (ii) the TPS scheme, starting from available data which are employed as conditioning information, as described in Section 2. Section 3 reports details about the numerical approach adopted. Section 4 presents the statistical analysis (in terms of mean, variance, covariance function and probability distribution) of hydraulic heads as a function of (i) location in the domain and (ii) methodology of geological reconstruction of the system, highlighting the competing effect of the source term and boundary conditions. Since typical head observations are collected within screened boreholes, we explore the extent to which vertically averaging hydraulic heads can retain qualitative and quantitative information on the statistical behavior of point-wise head values.

## 2. Lithological database and hydro-facies simulation strategy

The numerical investigation is performed on a numerical model that is patterned after a lithological database and geological information which are associated with a groundwater system located between Adda and Serio Rivers in the Lombardia region, Italy (see Fig. 1).

Geological surveys and drillings have been performed in the area and a rich lithological dataset is available together with detailed geological descriptions. The data upon which our synthetic simulations of litho-type distributions are based correspond to a dense network of boreholes (approximately 1 borehole/2.3 km$^2$). Fig. 1 depicts a sketch of the area where these data have been collected. We refer to Bianchi Janetti et al. (2011), Vassena et al. (2012) and references therein, for thorough reviews about the geological setup, the main hydrogeological features of the system and the detailed description of available data.

A preliminary analysis has been performed to properly code the information within readily accessible databases containing well identification codes, geo-referenced coordinates, location, thickness and depth of recorded stratigraphic levels, as well as detailed lithological description. Data re-classification is performed to obtain a realistic (albeit simplified) representation of the complex and heterogeneous architecture that is inherent to the observed aquifer system. The various hydro-facies detected in the region are classified and described in terms of five categorical variables, or indicators, i.e., fine-grained materials (F1), sand (F2), gravel (F3), compact conglomerates (F4), and fractured conglomerates (F5).

Two FRM methods are selected, an indicator-based approach (SISIM) and the Truncated Plurigaussian Simulation method, to simulate three-dimensional Monte Carlo conditional hydro-facies distributions within the sub-domain depicted in Fig. 1c.

Details of the geospatial analyses of the indicator-transformed hydro-facies classes are presented in the following. As recalled in Section 1, the TPS method is based on the simulation of multiple Gaussian random functions to allow for complex litho-type spatial arrangements embedding contact rules (termed litho-type rules) based on field observations and interpretations. Indicator (cross-) covariances are related to the (cross-) covariances of the underlying Gaussian random functions embedded in the TPS technique thus allowing a consistent comparison between the two procedures here adopted.

The five identified hydro-facies are associated with proportions of 43.6% (F1), 1.8% (F2), 22.3% (F3), 21.2% (F4), and 11.1% (F5). The fine-grained sediments are included in class F1 and their occurrence marks the regular/cyclic depositional sequences which are typical of a fluvial system. The vertical distribution of facies proportions estimated from the complete available data-set shows that the material proportions are not uniform along the vertical direction: gravel (F3) is dominant at the highest elevations while conglomerates (F5) and fine-grained materials (F1) largely populate the bottom of the aquifer. Fig. 2a depicts the litho-type contact rule which is derived from the analysis of the geological setting and data in the area. This rule embeds a quantitative analysis of the number of contact occurrences between the five hydro-facies. The fine hydro-facies F1, which is the most abundant in the system, is in contact with all the remaining materials. The other four classes are in contact with each other following a grain-size hierarchy.

A detailed geospatial analysis of the indicator-based variables is performed and three principal anisotropy directions are identified (North–South, N–S; West–East, W–E; and vertical). This finding is consistent with field observations and lithological interpretations for the area where, e.g., the river network, and therefore the depositional trends, is aligned along the N–S direction. Table 1 summarizes the parameters of the exponential indicator variograms which are estimated on the basis of their empirical counterparts and are adopted for the SISIM simulations. The selection of the exponential model has been based on the least square criterion and standard analysis of cross-validation errors (details not
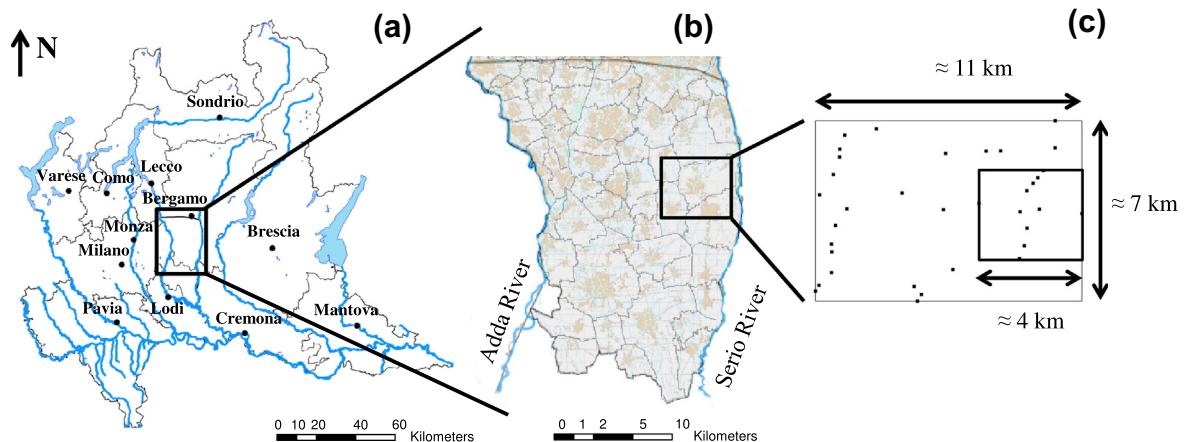


**Fig. 1.** Sketch of the area from which sedimentological data are extracted including (a) Lombardia region in Italy, the location of (b) the large scale aquifer system studied by Bianchi Janetti et al. (2011) and (c) the sub-domain where conditional litho-facies simulations are performed (delimited by a rectangle) together with the local borehole network.
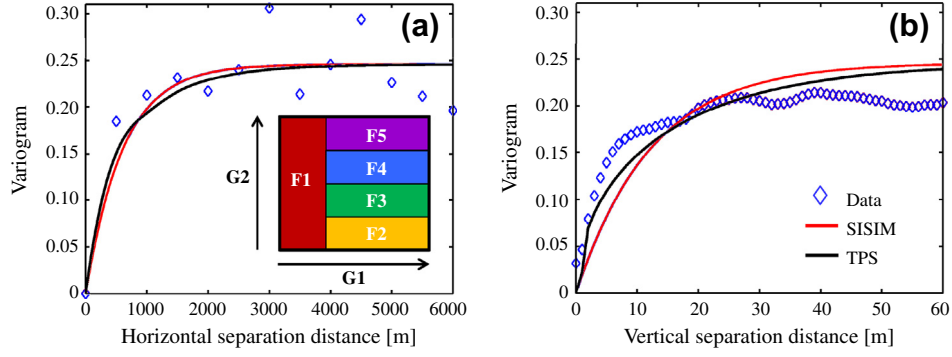
**Fig. 2.** Experimental (symbols) and modeled (SISIM and TPS) variograms for facies F1 along (a) N–S and (b) vertical directions. The sketch of the litho-type rule adopted for the TPS scheme is embedded as an inset.

**Table 1**
Indicator variogram model parameters estimated for the five hydro-facies. A zero nugget is estimated for all models.

| Lithology class | Sill | Ranges [m] – SISIM (N–S/W–E/vertical) |
|---|---|---|
| F1 | 0.246 | 1830/1280/37 |
| F2 | 0.017 | 700/470/20 |
| F3 | 0.173 | 1240/910/34 |
| F4 | 0.167 | 860/670/20 |
| F5 | 0.098 | 1220/900/36 |

reported). An exponential model is also selected to characterize the structure of the spatial dependence of the two underlying Gaussian fields employed in the TPS method. The parameters of the variograms of these fields are estimated through the iterative procedure presented by Emery (2007). This procedure is based on an analytical relationship (see (3)–(6) in Emery, 2007) between the correlograms of the two Gaussian fields (G1, and G2) and the indicator variograms which are derived from the available data and employed in the SISIM-based simulation strategy. This analysis leads to estimating the range values of 900 m and 600 m, respectively along N–S and W–E directions, for both Gaussian fields. Vertical ranges of 19 m and 36 m are estimated for G1 and G2, respectively. As an example of the quality of the results obtained, Fig. 2 depicts selected directional sample indicator variograms associated with facies F1 together with the corresponding calibrated models adopted for the SISIM and TPS simulation techniques. It is noted that the available data density contributes to render estimates of horizontal ranges which are subject to more uncertainty than their vertical counterparts.

A number $N = 1000$ of three-dimensional realizations of hydro-facies distributions are generated with TPS and SISIM schemes. Indicator-based conditional simulations are performed via the software SISIM (Deutsch and Journel, 1997). TPS simulations are based on the algorithms and codes presented by Xu et al. (2006) and Emery (2007). For the purpose of our analysis and for reason related to computational costs, the numerical simulations are performed within a model domain whose extent corresponds to the sub-domain identified in Fig. 1c. The lithological and geological information available in this region are employed as conditioning data for our model aquifer system. The Cartesian grid adopted for the hydro-facies simulations comprises $74 \times 86$ elements, respectively along the N–S ($y$) and W–E ($x$) directions. The grid spacing is set to $\Delta x = \Delta y = 50$ m resulting in a simulation domain with a planar extent of $3700 \times 4300$ m$^2$. Since one of the objectives of this study is to analyze the way the vertical variability of hydraulic heads is impacted by facies distribution, boundary conditions and/or source terms without considering the effect of the particular geometry of the bottom of the aquifer, we adopt in the following a constant thickness $B = 100$ m which is representative of an average width of the system in the area. We discretize $B$ into 50 layers of uniform thickness $\Delta z = 2$ m for the purpose of our computations.

As an example, Fig. 3 shows two selected simulations, respectively obtained with SISIM and TPS. Both hydro-facies reconstruction methods reproduce the anisotropy pattern detected in the system. However, TPS renders an improved continuity of sedimentary structures, which are elongated along the N–S direction, consistent with observations from surface lithological maps. Table 2 lists the material volumetric proportions inferred from the available data and employed in the simulations. The sample average and standard deviation of the volumetric proportions calculated for each facies and for both simulation methods are also reported. The information is complemented by Fig. 4, which illustrates the rate of convergence of mean and standard deviation of the
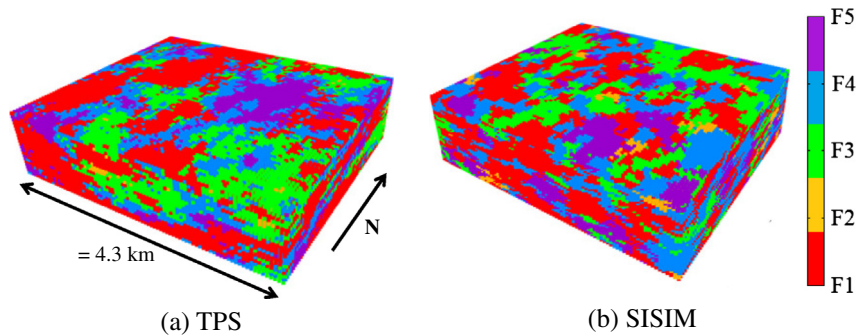


(a) TPS                    (b) SISIM

**Fig. 3.** Selected realizations of hydro-facies distributions obtained by means of (a) TPS and (b) SISIM. The size of the represented simulation domains is 3.7 km × 4.3 km × 0.1 km. Vertical exaggeration is set to 10× for ease of illustration.

| Hydro-facies | Input hydro-facies proportions (%) | $\mu_{SISIM}$ (%) | $\sigma_{SISIM}$ (%) | $\mu_{TPS}$ (%) | $\sigma_{TPS}$ (%) |
|---|---|---|---|---|---|
| F1 | 43.6 | 39.8 | 1.7 | 46.1 | 8.6 |
| F2 | 1.8 | 2.2 | 0.5 | 1.6 | 1.4 |
| F3 | 22.3 | 22.4 | 1.5 | 22.0 | 6.0 |
| F4 | 21.2 | 23.7 | 1.4 | 20.6 | 4.3 |
| F5 | 11.1 | 11.9 | 1.2 | 9.7 | 4.4 |

volumetric proportion of facies F1 and F4 through the Monte Carlo procedure. The collections of 1000 realizations provide relatively stable first and second moments of volumetric proportions of hydro-facies for both generation schemes. We note that sample statistics appear to converge slightly faster for the SISIM- than for the TPS-based simulations, the latter being characterized by a significantly larger variance than the former. Qualitatively and quantitatively similar results were obtained for the remaining facies. This is related to the increased degree of structured heterogeneity which is embedded in the conceptual model underlying TPS. In fact, in this case, the occurrence of a given facies at a location is accompanied by the appearance of other facies in the surrounding blocks in compliance with the adopted contact rule. This tends to enhance the variability of proportions across realizations and lowers the rate of convergence of the moments analyzed. Table 2 shows that the (ensemble) mean volumetric proportion values of hydro-facies occurrence calculated with both simulation schemes are close to the input values, the TPS-based sample displaying a relatively large variability across the realizations as reflected in the values of the associated coefficients of variation. These coeffi-
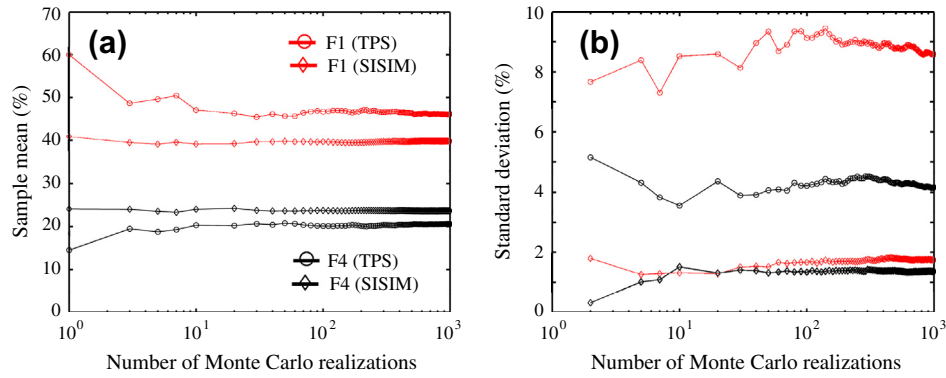


**Fig. 4.** Dependence of sample (a) mean and (b) standard deviation of the volumetric proportions of hydro-facies F1 and F4 on the number of Monte Carlo realizations for the SISIM- and TPS-based generation schemes.
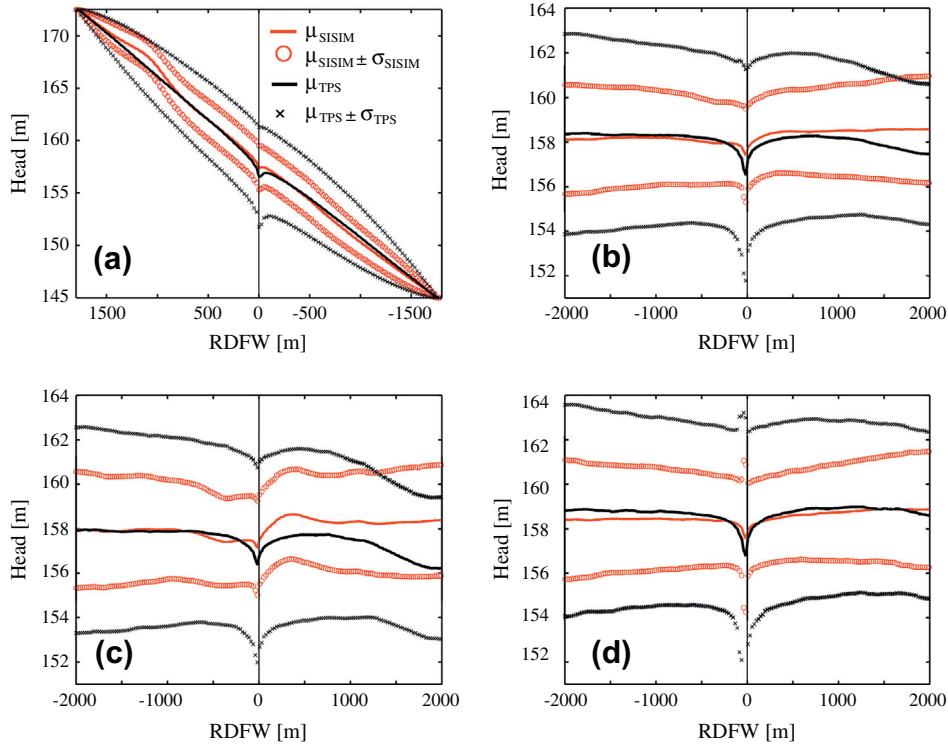


**Fig. 5.** Spatial dependence of Monte Carlo-based sample mean ($\mu_i$; i = SISIM, TPS) of hydraulic heads calculated through SISIM and TPS. Results are associated with vertical averaging of heads over the entire thickness of the domain along the (a) N–S and (b) W–E direction and with averaging over the (c) upper and (d) lower 20-m screened segments along the W–E direction. Intervals of width corresponding to one standard deviation ($\sigma_i$) around the corresponding sample means are also shown.
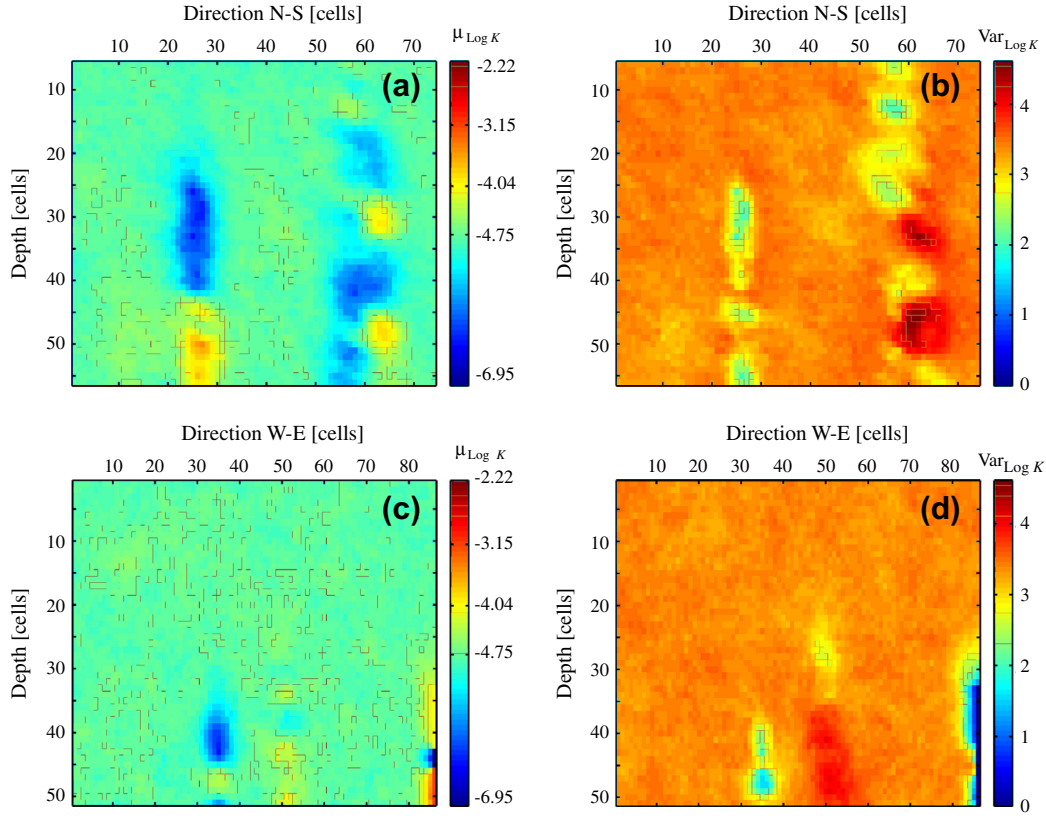
**Fig. 6.** SISIM-based vertical distributions of sample (a), (c) mean ($\mu_{LogK}$) and (b), (d) variance ($\text{Var}_{LogK}$) of the decimal logarithm of hydraulic conductivities, Log K, obtained along the two cross-sections represented in Fig. 5a and b. Vertical exaggeration is set to 25× for ease of visualization.
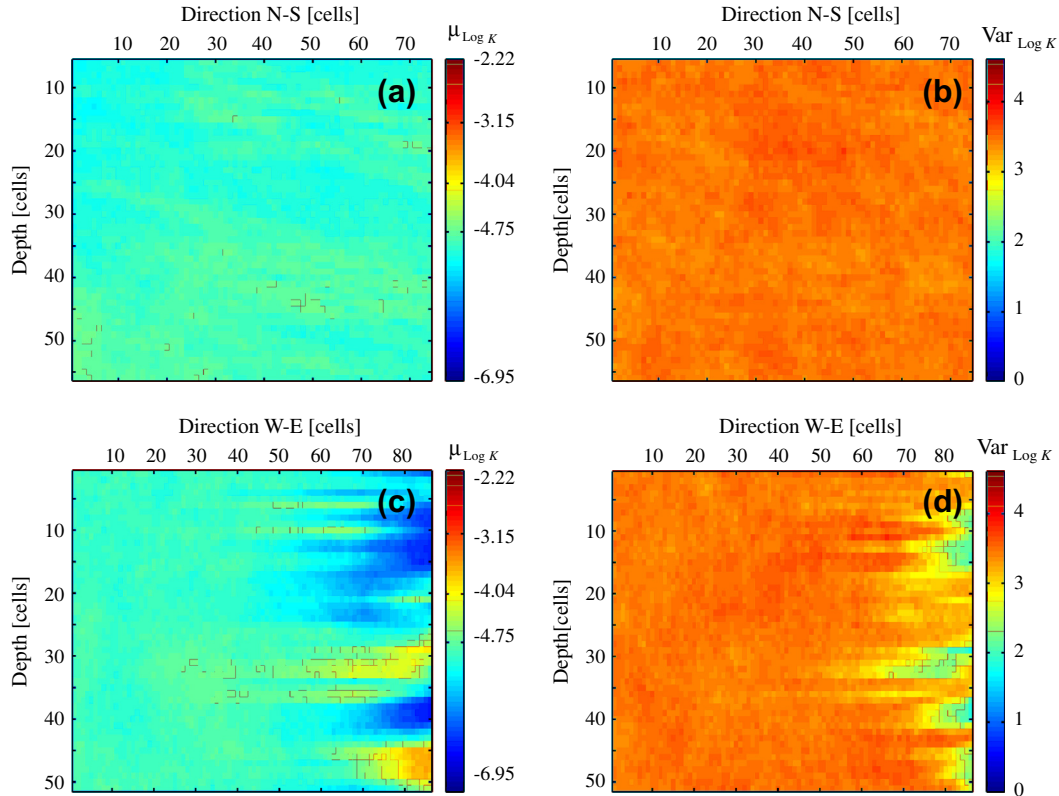


**Fig. 7.** TPS-based vertical distributions of sample (a), (c) mean ($\mu_{LogK}$) and (b), (d) variance ($\text{Var}_{LogK}$) of the decimal logarithm of hydraulic conductivities, Log K, obtained along the two cross-sections represented in Fig. 5a and b. Vertical exaggeration is set to 25× for ease of illustration.
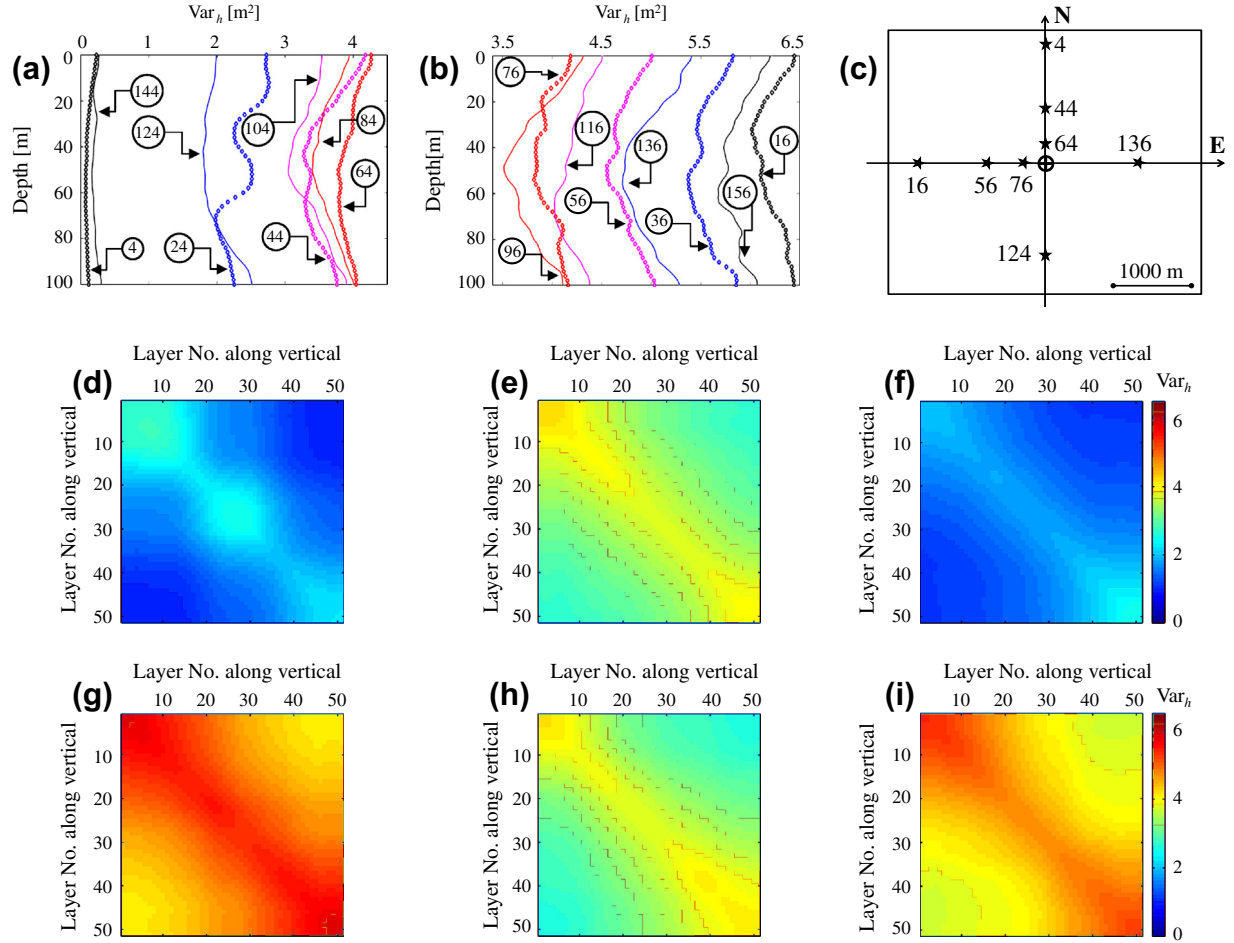
**Fig. 8.** (a and b) Vertical distributions of the variance of point values of hydraulic heads ($Var_h$) at different planar control points (marked by circled numbers) and calculated from the SISIM-based simulations. Planar location of some of the control points is illustrated in (c) as a guidance. Covariance matrices of point values of hydraulic heads at diverse depths (along the vertical direction) taken at the control points (d) 24, (e) 64, (f) 124, (g) 36, (h) 76 and (i) 136.

cients vary between 0.19 (for F1) and 0.88 (for F2) and are generally larger than those associated with the SISIM scheme, which range between 0.04 (for F1) and 0.22 (for F2). Moreover, the values of standard deviation associated with the sample mean proportions, computed as $\sigma_j / \sqrt{N}$ ($j \in$ {SISIM, TPS}), suggest that only the target (input) volumetric proportions of F3 for SISIM and of F2 and F3 for TPS are comprised within intervals of width equal to $\pm 3\sigma_j / \sqrt{N}$ around the corresponding sample mean. The apparent inability of the two methods to reproduce exactly the target volumetric proportions of hydro-facies for each realization of the collection might be related to the low relative proportion (which is lower than 2.3%) between the conditioning data ($\approx 7.50 \times 10^3$) and the high number of simulated values ($\approx 3.25 \times 10^5$). This is specifically critical for the horizontal direction, where, as typically observed in practical applications, the spacing between data locations is larger than that associated with the vertical direction. However, the results listed in Table 2 can be considered satisfactory for the purposes of our synthetic study. A significant relative error ($\approx 20\%$) can be observed only for the SISIM-based reconstruction of the less abundant hydro-faces (F2). In general, the average volumetric proportions based on TPS are closer to the input values than the SISIM-based counterparts. The sample pdf of the hydro-facies proportions evaluated on the basis of the 1000 MC simulations is approximately Gaussian (details not shown) for all litho-types considered through the SISIM-based realizations. With reference to the TPS method, it is noted that the generated distributions of F2 and F5 (the less abundant indicator classes) are associated

with clear non-Gaussian behavior, with significant positive skewness and heavy tails associated with large volumetric proportions.

## 3. Numerical simulations of head distributions

The numerical mesh employed for the flow simulations is built by further refinement of the hydro-facies generation grid along the horizontal directions, resulting in a regular horizontal grid spacing of $\Delta x' = \Delta y' = \Delta x / 2 = 25$ m. The vertical discretization grid adopted for the flow simulations coincides with the one adopted for the hydro-facies generation procedure, i.e. $\Delta z' = \Delta z = 2$ m. The generated sample of stochastic realizations of (conditional) three-dimensional hydro-facies distributions are employed to simulate a steady-state convergent flow scenario due to pumping. The flow problem is solved through the code MODFLOW (McDonald and Harbaugh, 1988). Noting that at the large field scale of investigation the spatial arrangement of litho-types is a key driver for the distribution of groundwater flow quantities, we adopt here a composite medium approach (Winter et al., 2003) where the spatial location of facies is uncertain and their hydraulic attributes are deterministically known. We set the following values for hydraulic conductivity $K_{Fi}$ associated with facies $F_i$ ($i = 1, ..., 5$): $K_{F1} = 1.12 \times 10^{-7}$ m/s, $K_{F2} = 1.79 \times 10^{-5}$ m/s, $K_{F3} = 7.16 \times 10^{-4}$ m/s, $K_{F4} = 9.09 \times 10^{-5}$ m/s, and $K_{F5} = 6.05 \times 10^{-3}$ m/s. These values are inferred from the results of geostatistical inverse modeling of the large scale groundwater system depicted in Fig. 1 (Bianchi Janetti et al., 2011) and are used here for consistency. A fully penetrating
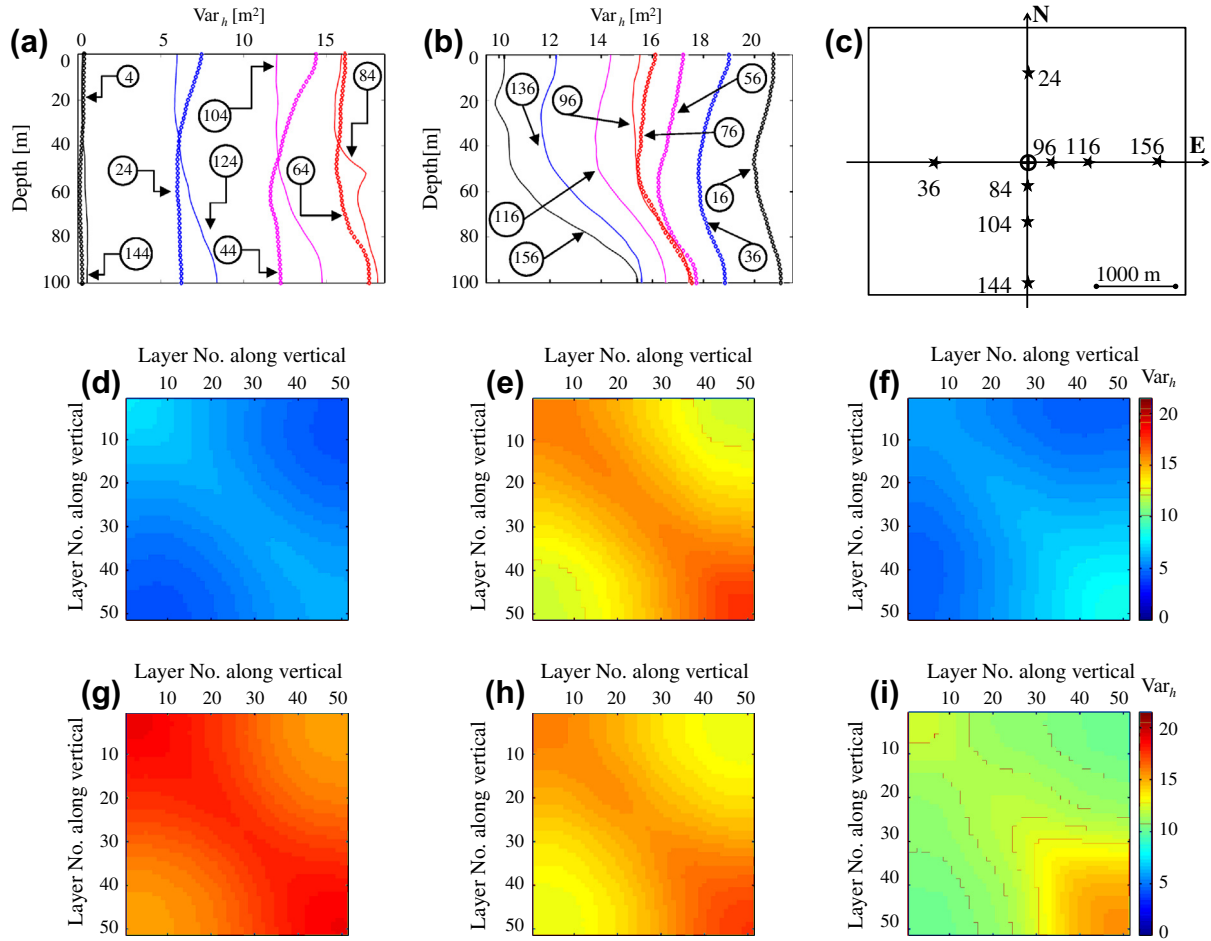
**Fig. 9.** (a and b) Vertical distributions of the variance of point values of hydraulic heads (Var$_h$) at different planar control points (marked by circled numbers) and calculated from the TPS-based simulations. Planar location of some of the control points is illustrated in (c) as a guidance. Covariance matrices of point values of hydraulic heads at diverse depths (along the vertical direction) taken at the control points (d) 24, (e) 64, (f) 124, (g) 36, (h) 76 and (i) 136.

pumping well is located approximately at the center of the domain. A total pumping rate of 3000 m³/day is imposed and subdivided among the well blocks, proportionally to the hydraulic conductivity of each block. Uniform heads of 172.5 m and 145 m are respectively imposed on the northern and southern edges of the domain to mimic typical average values of regional hydraulic gradients observed in the area (≈0.7%). No-flow conditions are imposed along the eastern, western, top and bottom boundaries. The results of the three-dimensional flow modeling are taken to simulate sets of drawdown responses monitored at a set of vertical observation boreholes. These enable one to compare the effect of the stochastic simulation schemes on the response of the system, in terms of hydraulic head statistics.

Statistical analysis of calculated hydraulic heads is performed in terms of low-order moments (mean and co-variance) and probability density functions (pdfs) by considering point and vertically averaged values. The latter are evaluated along segments of thickness ΔB = 10 m, 20 m and 100 m (i.e., corresponding to 1/10 B, 1/5 B, and B, the complete thickness of the domain), to simulate completely and partially screened borehole readings.

## 4. Results

Fig. 5 illustrates the spatial distribution along selected cross sections of the sample mean hydraulic heads calculated for both simulation methods. Results are reported in terms of radial

distance from the well (RDFW; positive for points located North or East of the pumping well and negative otherwise) and are obtained by vertical averaging point heads over (i) the complete domain thickness (Fig. 5a and b) and (ii) the upper (Fig. 5c) and lower (Fig. 5d) 20-m screened segments. Intervals of width corresponding to one standard deviation are reported to provide an indication of the extent of the sample variability induced by the generation method. Regardless the width of the selected vertical integration segment, it is noted that hydraulic head values are highest for SISIM in the northern and eastern sub-regions of the simulation domain. On the other hand, TPS renders largest average values in the southern and western parts of the system. The largest drawdown at the well is always obtained from the TPS method. TPS yields the largest sample standard deviation of hydraulic heads, consistent with the results illustrated in Table 2. The observed behavior can be related to the differences in the internal structure of the hydro-facies and hydraulic conductivity distributions generated with the two selected methodologies. To illustrate this, Fig. 6 depicts vertical distributions of SISIM-based sample mean and variance of the decimal logarithm of hydraulic conductivities, Log K, obtained along the two cross-sections represented in Fig. 5a and b. Fig. 7 shows corresponding results obtained from the TPS-based simulations. The cross-sections depicted in Figs. 6 and 7 do not contain conditioning data. It is noted that for these sections the SISIM-based scenario appears to be associated with a more pronounced impact of the lithological information available at the
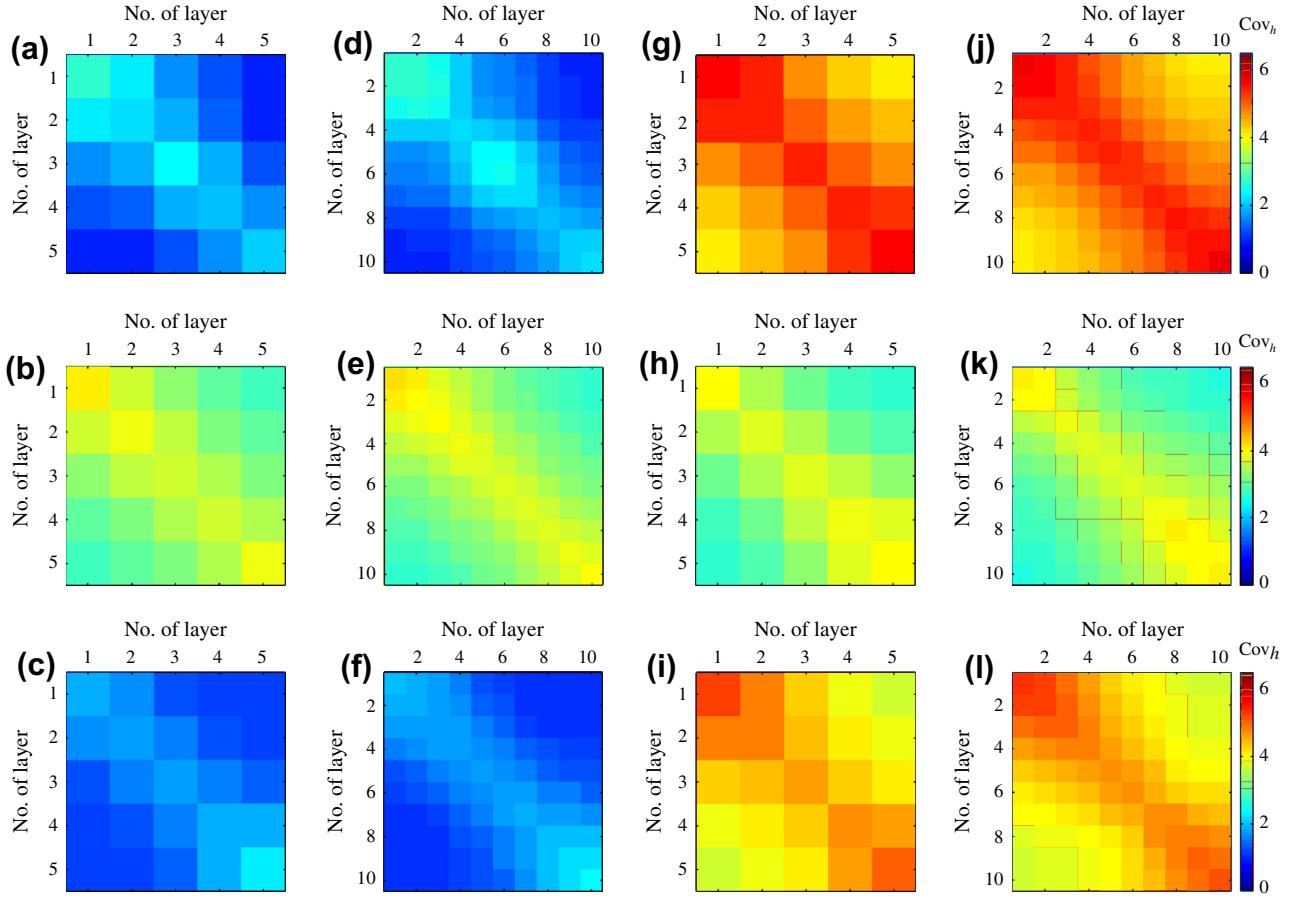
**Fig. 10.** SISIM-based covariance matrices of hydraulic heads (Cov$_h$) at diverse depths along verticals taken at selected control points (a and d) 24, (b and e) 64, (c and f) 124, (g and j) 36, (h and k) 76 and (i and l) 136 (see Figs. 8c and 9c for location of control points). Results correspond to two diverse degrees of refinement of the vertical averaging thickness, i.e., $\Delta B = 10$ m (Fig. 10d–f and j–l) and $\Delta B = 20$ m (Fig. 10a–c and g–i). Horizontal and vertical axes represent the layer numbering associated with each averaging interval.

conditioning points than TPS-based results are, where the effect of the selected litho-type contact rule is superimposed to the impact of the conditioning points.

Along the N–S direction the SISIM method yields persistent clusters characterized by small ($\approx 10^{-7}$ m/s) and large ($\approx 10^{-4}$ m/s) conductivity values while the TPS-based results are associated with a relatively uniform ($\approx 10^{-5}$ m/s) $K$ distribution and a large Log $K$ variance. This observation is consistent with the quite regular behavior displayed in Fig. 5a by the TPS-based mean head ($\mu_{TPS}$) and its large associated variance, when compared to the corresponding moments estimated on the basis of SISIM. A different behavior is noted along the W–E direction where a relatively uniform mean Log $K$ distribution associated with SISIM is replaced by a series of elongated structures honoring jointly the conditioning data and the imposed contact rule adopted for the TPS simulation scheme. As a consequence, while the mean head profile based on SISIM is approximately symmetric around the well in Fig. 5b, the TPS results are characterized by large drawdowns in the eastern part of the domain where there is the occurrence of elongated structures associated with small Log $K$ (Fig. 7c).

A key difference between the fields of Log $K$ sample variance obtained with the two methods lies in the relatively uniform distribution of persistently large values which is visible in the TPS results. This is opposed to the outcome of SISIM simulations, which are associated with a spatially heterogeneous pattern, alternating low and large variance values. The effect of the conditioning data on the spatial persistence of variance values is different for the two methodologies, due to the geological constraints imposed in

the TPS procedure through the adopted contact rules. These results are consistent with the spatial pattern which can be detected for single realizations of hydro-facies distributions.

Fig. 8 shows the vertical distribution of the variance of point values of $h$ at various relative distances from the well along N–S (Fig. 8a) and the W–E (Fig. 8b) directions and calculated from the SISIM-based simulations. Vertical profiles obtained at points located at the same radial distance from the well (see also Figs. 8c and 9c for the planar location of control points) are reported with the same color. Images of the covariance matrices of point values of heads at diverse depths along verticals taken at selected control locations complement the set of results (Fig. 8d–i). Fig. 9 depicts the corresponding quantities associated with TPS-based simulations.

With reference to the SISIM-based scenario, the variance of point values of $h$ forms non-uniform vertical profiles which are almost symmetric around the intermediate depth of the system ($z = 50$ m, see Fig. 8a and b). Differences between values of variance at the top and bottom of the aquifer are mainly related to the conditional nature of the simulations. The largest values of variance occur at locations close to the well and to the impervious boundaries (including the top and the bottom of the aquifer). Head variance tends to decrease and its vertical profile to become more uniform with increasing relative distance from the extraction well measured along the mean flow direction. This result is similar to what observed by Guadagnini et al. (2003) on the basis of their analytical solution of flow moment equations for bounded three-dimensional Gaussian (natural) Log $K$ fields under mean radial flow

conditions. Note that along the W–E direction the variance tends to first decrease and then to increase with distance from the well and reaches a local maximum at the no-flow boundaries. The qualitatively observed increase in the correlation between hydraulic head values at mid locations along the vertical which is observed in Fig. 8d and the wavy behavior noted for the vertical distribution of variance values in Fig. 8a are consistent with the persistence of clusters of fine materials in the area stemming from the SISIM generation method (Fig. 6).

The variance distributions associated with the TPS method are typically characterized by a reduced vertical variability at locations along the N–S direction (see Fig. 9a) and generally display larger values than those associated with SISIM-based results (compare Figs. 8a and 9a). Moving along the W–E direction (see Fig. 9b), it is noted that the variance associated with locations at the bottom of the system is consistently larger than that related to points close to the top. These effects are due to the imposed contact rules between hydro-facies. These rules tend to reproduce the natural dip of the geological structures in the system and increase the possibility of occurrence of vertical fluxes. As noted in Section 2 for the reconstruction of the litho-types distributions, the imposed contact rules tend to increase the internal variability of the system and result in a negative impact on the predictability of hydraulic heads which tend to be characterized by large variances. The general behavior of the covariance matrix calculated between point values of hydraulic heads is qualitatively similar for the two simulation methods (see Figs. 8 and 9d–i). A strong non-stationary behavior and heterogeneous distribution of typical scales of head correlation can be qualitatively inferred from Figs. 8 and 9. Regardless of the generation scheme, along the mean flow direction (N–S) the rate of decrease of the vertical covariance of $h$ appears to increase (thus suggesting a decrease of vertical correlation scales) with increasing

distance from the pumping well (see Figs. 8d–f and 9d–f). On the other hand, along the W–E direction, perpendicular to the mean base flow, the generation scheme strongly influences the correlation structure of $h$. SISIM-based results suggest a degree of vertical correlation of $h$ that tends to increase with the distance from the pumping well (see Fig. 8g–i). TPS-based outcomes are not prone to an immediate interpretation. The degree of vertical correlation of hydraulic heads appear to be higher at locations in the western than in the eastern region, consistent with the occurrence of elongated structures in the latter region and the almost uniform distribution of Log$K$ along the western area (Fig. 7c). A corresponding analysis (details not reported) revealed that (integrated and point-wise) hydraulic head values display an increased degree of horizontal correlation along the direction perpendicular to mean flow and when a SISIM rather than a TPS approach is used. It is also noted that the horizontal head covariance tends to display the slowest rates of decay (thus suggesting relatively large horizontal correlation scales) for reference points located close to the impervious (horizontal and vertical) boundaries. These types of results can be useful during typical statistical analyses of monitored $h$ values, which are often performed assuming that variables are uncorrelated in space. Our study shows that this latter assumption is roughly satisfied only when considering points which (a) lie along the mean direction of the system base flow, and (b) are located relatively far from the source terms.

Examples of quantitative results on the effect that vertical averaging of hydraulic heads along diverse depth intervals can have on the vertical correlation structure are reported in Fig. 10. The figure displays SISIM-based covariance matrices of hydraulic heads at diverse depths along verticals taken at three selected control points along the N–S (Fig. 10a–f) and W–E (Fig. 10g–l) directions and corresponding to two different degrees of refinement of the vertical
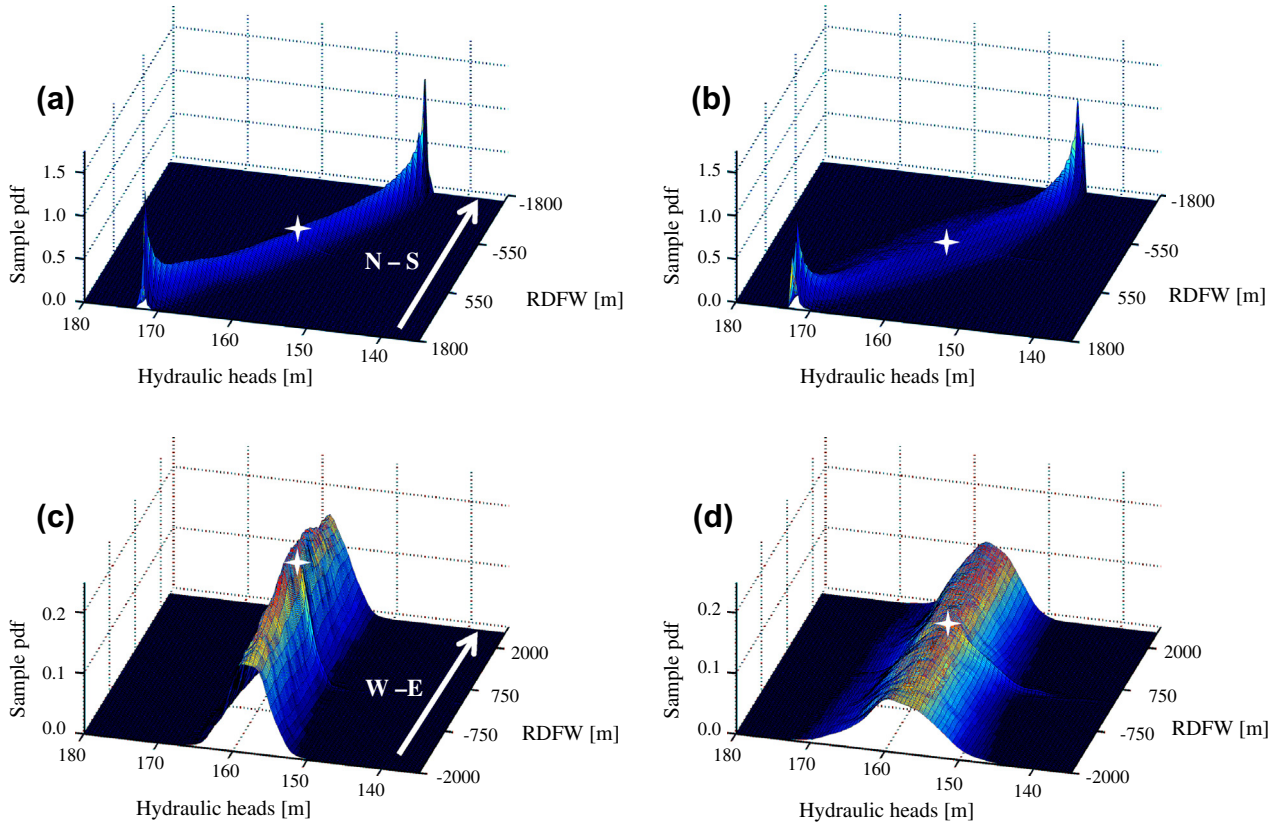


**Fig. 11.** Spatial distribution of the sample pdf of vertically integrated hydraulic heads calculated through the (a), (c) SISIM- and (b), (d) TPS-based reconstruction methods along the N–S (a)-(b) and W–E (c)-(d) directions. White stars mark the location of the pumping well.

averaging thickness, i.e., $\Delta B = 20$ m (Fig. 10a–c and g–i) and 10 m (Fig. 10d–f and j–l). Despite the loss of resolution and information along the vertical direction due to spatial averaging, the main representative features and patterns observed for point-values based covariances (see Fig. 8d–i) remain visible. The same observation can be made for TPS-based simulations (not shown).

Fig. 11 depicts the N–S and W–E spatial dependence of the sample pdf of hydraulic heads averaged over the whole aquifer thickness and calculated through the SISIM- and TPS-based reconstruction methods. The SISIM-based setting appears to be associated with the largest peakedness of the empirical distributions. Visual inspection of sample pdfs suggests that a Gaussian model might not always be appropriate to characterize the observed behavior. These pdfs are sometimes characterized by heavy tails, for which, e.g., an $\alpha$-stable distribution might be an appropriate interpretive model. On this basis, hydraulic head values calculated at diverse locations in the system and averaged along vertical segments of various thicknesses are examined by (a) assuming that they derive from an $\alpha$-stable distribution, (b) estimating the parameters of these distributions, and (c) analyzing the degree to which the calibrated distributions fit the numerical results.

We recall that an $\alpha$-stable distribution is described by four real-valued parameters: stability index $\alpha \in (0,2]$, skewness $\beta \in [-1,1]$, scale $\sigma > 0$ and shift $\mu$. The following parameterized form, described by Samorodnitsky and Taqqu (1994), is applied to define the log characteristic function of an $\alpha$-stable variable, $X$:

$$\ln\langle e^{i\phi X}\rangle = i\mu\phi - \sigma^\alpha |\phi|^\alpha [1 + i\beta \text{sign}(\phi)\omega(\phi,\alpha)];$$
$$\omega(\phi,\alpha) = \begin{cases} -\tan\frac{\pi\alpha}{2} & \text{if} \quad \alpha \neq 1 \\ \frac{2}{\pi}\ln|\phi| & \text{if} \quad \alpha = 1 \end{cases} \tag{1}$$

Here, $\langle\rangle$ indicates the expected value (ensemble mean), $\phi$ is a real-valued parameter and $\text{sign}(\phi) = 1, 0, -1$ if $\phi > 0$, =0, <0, respectively. The optimal estimated values $\hat{\theta} = (\hat{\alpha}, \hat{\beta}, \hat{\sigma}, \hat{\mu})$ of the parameters array $\theta = (\alpha, \beta, \sigma, \mu)$ are obtained through the maximum likelihood (ML) approach upon maximizing the likelihood:

$$l(\theta) = \sum_{i=1}^{n} \log f(X_i|\theta) \tag{2}$$

with respect to $\theta$, $n$ and $f(X|\theta)$ respectively being the sample size and the conditional probability density function of $X$. ML is implemented through the program STABLE (Nolan, 2001) that provides reliable estimates of stable densities for $\alpha > 0.1$. A Gaussian distribution is recovered when $\alpha = 2$.

A statistical analysis is then performed at selected locations to test the influence of the averaging procedure along the vertical direction on the simulation results. As an example, Fig. 12 illustrates the variability along the vertical of SISIM-based hydraulic head sample pdfs calculated on the basis of the Monte Carlo simulations at control point 24 (located in the northern part of the domain, at about 600 m from the prescribed hydraulic head boundary and 1250 m from the well, see Fig. 9c) and for the diverse averaging intervals considered, i.e. point values (Fig. 12a), $\Delta B = 10$ m (Fig. 12b) and $\Delta B = 20$ m (Fig. 12c). The influence of the northern (prescribed head) boundary condition is notable on the skewness and on the (left) heavy tail of the distributions. The point-wise and vertically averaged values of $h$ share some notable statistical properties. All sample distributions appear to be reasonably fitted by an $\alpha$-stable model which is negatively skewed (i.e., $\hat{\beta} \approx -1.0$) and with $\hat{\alpha}$ values ranging between 1.6 and 1.8. The same analysis performed at points lying in the southern part of the system provides qualitatively similar results, with sample pdfs being fitted by positively skewed ($\hat{\beta} \approx 1.0$) $\alpha$-stable distributions. TPS-based results display an analogous behavior (not shown) albeit characterized by generally longer tails (with estimates $\hat{\alpha} \approx 1.5$). The tails of the hydraulic heads pdfs along
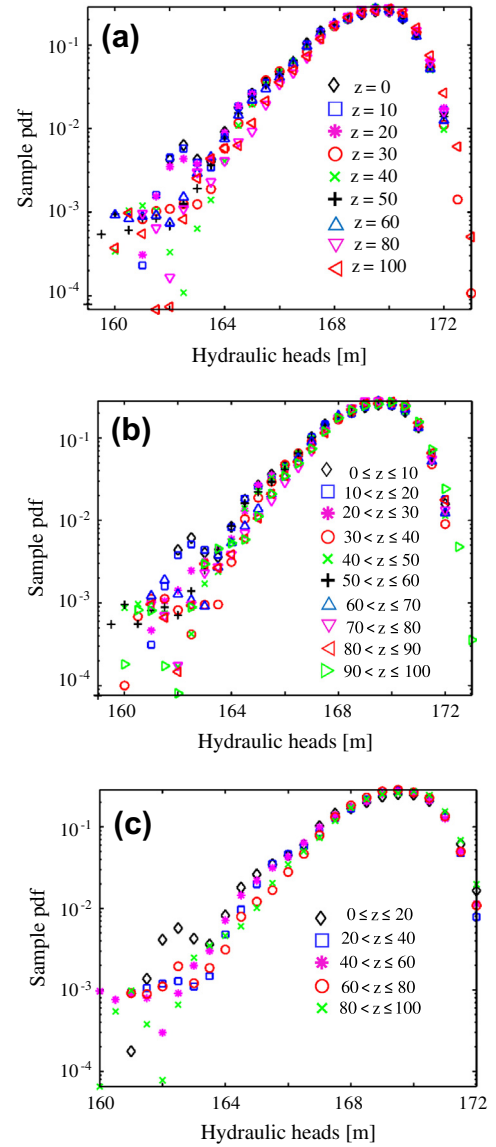


**Fig. 12.** Vertical distribution of SISIM-based hydraulic head sample pdfs calculated at control point 24 (see Fig. 9c for location of the control point) and for the diverse averaging intervals considered, i.e., (a) point hydraulic head values, and vertically averaged heads with (b) $\Delta B = 10$ m and (c) $\Delta B = 20$ m.

the N–S direction become increasingly evident for both simulation schemes, and hence best interpreted through an $\alpha$-stable distribution, as the distance from the pumping well increases and the (deterministic Dirichlet) boundaries are approached. The observed similarities between the shapes of the sample pdfs of point-wise and vertically averaged heads suggests the possibility of capturing the key features of the statistical behavior of $h$ by means of vertically integrated observations. Tail oscillations which appear in the plots can be an artifact of the number of Monte Carlo iterations performed. In the presence of long-tailed pdfs, oscillations in the tails are visible even as a very large number of samples are considered (e.g., 100,000 samples, as shown for example by Guadagnini et al. (2012)). On the basis of our experience and prior work (e.g., Ballio and Guadagnini, 2004; Riva et al., 2006, 2008; Guadagnini et al., 2012 and references therein), the number of realizations here performed can be deemed as adequate to enable one to capture the key features and shape (albeit not all the details) of the target probability distributions.
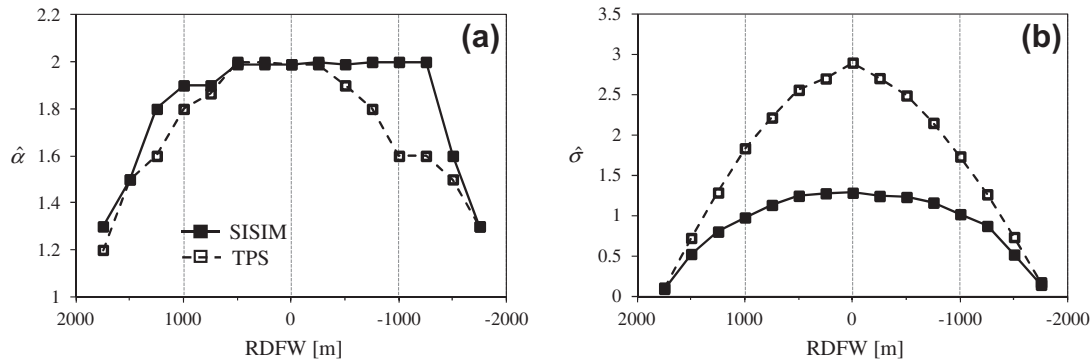
**Fig. 13.** Estimates of (a) stability index ($\hat{\alpha}$) and (b) scale parameter ($\hat{\sigma}$) of hydraulic heads integrated along the full aquifer thickness versus RDFW along the N–S direction.

Fig. 13a reports the N–S spatial dependence of estimates $\hat{\alpha}$ associated with the sample distributions of vertically averaged (over the complete thickness of the domain) hydraulic heads for both the SISIM- and TPS- based results. In general, we note that the tails of the head distributions are longer (i.e., $\hat{\alpha}$ is smaller) for TPS- than for SISIM- based simulations and decrease as the distance from the prescribed (deterministic) head boundaries increases. For large distances from these boundaries or close to the pumping well the distributions tends to become Gaussian (i.e., $\hat{\alpha} = 2.0$). At locations close to the fixed head boundaries, the distribution is skewed towards values which are representative of the inner portion of the domain.

Conversely, the pdfs of vertically averaged heads along the W–E direction appear to be well interpreted by the Gaussian model (i.e., $\hat{\alpha} \approx 2.0$), regardless the thickness of the vertical averaging segment and the generation model adopted (not shown). The prescribed flux boundary conditions introduce less constraints (through the Monte Carlo realizations) to the heads computed along the W–E direction and the shape of the sample head distributions is not significantly modified when approaching the boundaries.

Fig. 13b reports the N–S spatial dependence of estimates $\hat{\sigma}$ obtained for the distribution of vertically averaged hydraulic heads for both the SISIM- and TPS- based results. Since the scale parameter $\sigma$ is linked to the (ensemble) variability of the variable (in particular its square value is equal to half the variance when $\alpha = 2.0$), we observe an increase of $\hat{\sigma}$ with the distance from the fixed head boundaries. Consistent with the analysis presented above, $\hat{\sigma}$ is significantly larger for the TPS-based results than for their SISIM counterparts.

## 5. Conclusions

Our work leads to the following major conclusions.

1. Hydraulic heads deduced from TPS-based flow simulations exhibit larger variability than their counterparts evaluated by an SISIM-based modeling strategy. This is a consequence of the fact that setting geological contact rules, as considered within a TPS simulation scheme, can lead to an increased variability in the internal architecture of hydro-facies distributions within a relatively large-scale aquifer model of the kind we consider.
2. Covariance matrices and probability distributions of point and vertically averaged values of hydraulic heads display similar key representative features and patterns. Therefore, typical measurements taken in screened boreholes can be used to infer qualitative information about the correlation structure and the statistical properties of heads. The latter can then be employed within typical Probabilistic Risk Assessment procedures.

3. Probability distributions of heads close to prescribed head boundaries are skewed, show a long tailing behavior and are accurately fitted by α-stable distributions. The tails of the distributions are longer for TPS- than for SISIM- based results.
4. Probability distributions of heads close to impervious boundaries or to source terms (such as pumping wells) appear to be almost symmetric and reasonably well interpreted by Gaussian models.
5. Due to the enhanced degree of variability displayed within the collection of simulations and to the occurrence of long-tailed pdfs, reliance on a TPS scheme yields a broader range of possible drawdown values for the simulated groundwater system. As such, TPS-based results are associated with the most conservative (in terms of high extreme values) drawdown values which can then be related to a given threshold probability of occurrence in the context of PRA protocols where the target variable is piezometric drawdown.

## References

Ababou, R., McLaughlin, D., Gelhar, L.W., Tompson, A.F.B., 1989. Numerical simulation of three-dimensional saturated flow in randomly heterogeneous porous media. Transport Porous Med. 4 (6), 549–565.

Ballio, F., Guadagnini, A., 2004. Convergence assessment of numerical Monte Carlo simulations in groundwater hydrology. Water Resour. Res. 40, W04603. http://dx.doi.org/10.1029/2003WR002876.

Bellin, A., Tonina, D., 2007. Probability density function of non-reactive solute concentration in heterogeneous porous formations. J. Contam. Hydrol. 94 (1–2), 109–125. http://dx.doi.org/10.1016/j.jconhyd.2007.05.005.

Betzhold, J., Roth, C., 2000. Characterizing the mineralogical variability of a Chilean copper deposit using plurigaussian simulations. J. S. Afr. Inst. Min. Metall. 100 (2), 111–119.

Bianchi Janetti, E., Guadagnini, L., Riva, M., Larcan, E., Guadagnini, A., 2011. Geostatistical characterization of a regional scale sedimentary aquifer. In: Ubertini, F., Viola, E., de Miranda, S., Castellazzi, G. (Eds.), Prof. of XX Congresso dell'Associazione Italiana di Meccanica Teorica e Applicata, Bologna 12–15 September 2011, pp. 1–10 (ISBN 978-88-906340-1-7 (online)).

Bolster, D., Barahona, M., Dentz, M., Fernández-García, D., Sánchez-Vila, X., Trinchero, P., Valhondo, C., Tartakovsky, D.M., 2009. Probabilistic risk analysis of groundwater remediation strategies. Water Resour. Res. 45. http://dx.doi.org/10.1029/2008WR007551.

Carle, S.F., 1999. T-PROGS: transition probability geostatistical software version 2.1. University of California, Davis, CA.

Casar-González, R., 2001. Two procedures for stochastic simulation of vuggy formations. SPE Paper 69663, SPE, Richardson, TX.

Dagan, G., 1985. A note on higher-order corrections of the head covariances in steady aquifer flow. Water Resour. Res. 21 (4), 573–578.

Dagan, G., 1989. Flow and Transport in Porous Formations. Springer-Verlag, New York.

De Barros, F.P.J., Ezzedine, S., Rubin, Y., 2012. Impact of hydrogeological data on measures of uncertainty, site characterization and environmental performance metrics. Adv. Water Resour. 36, 51–64. http://dx.doi.org/10.1016/j.advwatres.2011.05.004.

Dell'Arcíprete, D., Bersezio, R., Felletti, F., Giudici, M., Comunian, A., Renard, P., 2012. Comparison of three geostatistical methods for hydro-facies simulation: a test on alluvial sediments. Hydrogeol. J. 20, 299–311. http://dx.doi.org/10.1007/s10040-011-0808-0.

Deutsch, C.V., Journel, A.G., 1997. GSLIB: Geostatistical Software Library and User's Guide, second ed. Oxford University Press, UK.

Dowd, P., Xu, C., Mardia, K.V., Fowell, R.J., 2007. A comparison of methods for the stochastic simulation of rock fractures. Math. Geol. 39 (7), 697–714.

Emery, X., 2004. Properties and limitations of sequential indicator simulation. Stoch. Env. Res. Risk. A 18, 414–424.

Emery, X., 2007. Simulation of geological domains using the plurigaussian model: new developments and computer programs. Comput. Geosci. 33, 1189–1201.

Englert, A., Vanderborght, J., Vereecken, H., 2006. Prediction of velocity statistics in three-dimensional multi-Gaussian hydraulic conductivity fields. Water Resour. Res. 42 (3), W03418. http://dx.doi.org/10.1029/2005WR004014.

Enzenhoefer, R., Nowak, W., Helmig, R., 2012. Probabilistic exposure risk assessment with advective dispersive well vulnerability criteria. Adv. Water Resour. 36, 121–132. http://dx.doi.org/10.1016/j.advwatres.2011.04.018.

Falivene, O., Arbués, P., Gardiner, A., Pickup, G., Muñoz, J.A., Cabrera, L., 2006. Best practice stochastic facies modeling from a channel-fill turbidite sandstone analog (the Quarry outcrop, Eocene Ainsa basin, northeast Spain). AAPG Bull. 90, 1003–1029.

Falivene, O., Cabrera, L., Muñoz, J.A., Arbués, P., Fernández, O., Sáez, A., 2007. Statistical grid-based facies reconstruction and modeling for sedimentary bodies. Alluvial-palustrine and turbiditic examples. Geol. Acta 5, 199–230.

Fiorotto, V., Caroni, E., 2002. Solute concentration statistics in heterogeneous aquifers for finite Peclet values. Transport Porous Med. 48 (3), 331–351. http://dx.doi.org/10.1023/A:1015744421033.

Galli, A.G., Beucher, H., Le Loc'h, G., Doligez, B., Heresim group, 1994. The Pros and Cons of the truncated Gaussian method. In: Armstrong, M., Dowd, P.A. (Eds.), Geostatistical Simulations. Kluwer Academic Publishers, Netherlands, pp. 217–233.

Guadagnini, A., Neuman, S.P., 1999a. Nonlocal and localized analyses of conditional mean steady state flow in bounded, randomly nonuniform domains 2. Computational examples. Water Resour. Res. 35 (10), 2999–3018. http://dx.doi.org/10.1029/1999WR900159.

Guadagnini, A., Neuman, S.P., 1999b. Nonlocal and localized analyses of conditional mean steady state flow in bounded, randomly nonuniform domains 1. Theory and computational approach. Water Resour. Res. 35 (10), 2999–3018. http://dx.doi.org/10.1029/1999WR900160.

Guadagnini, A., Riva, M., Neuman, S.P., 2003. Three-dimensional steady state flow to a well in a randomly heterogeneous bounded aquifer. Water Resour. Res. 39 (3), 1048. http://dx.doi.org/10.1029/2002WR001443.

Guadagnini, A., Neuman, S.P., Riva, M., 2012. Numerical investigation of apparent multifractality of samples from processes subordinated to truncated fBm. Hydrol. Process. 26 (19), 2894–2908. http://dx.doi.org/10.1002/hyp.8358.

Hernandez, A.F., Neuman, S.P., Guadagnini, A., Carrera, J., 2006. Inverse stochastic moment analysis of steady state flow in randomly heterogeneous media. Water Resour. Res. 42, W05425. http://dx.doi.org/10.1029/2005WR004449.

Jones, L., 1990. Explicit Monte Carlo simulation head moment estimates for stochastic confined groundwater flow. Water Resour. Res. 26 (6), 1145–1153. http://dx.doi.org/10.1029/WR026i006p01145.

Jurado, A., De Gaspari, F., Vilarrasa, V., Bolster, D., Sánchez-Vila, X., Fernández-García, D., Tartakovsky, D.M., 2012. Probabilistic analysis of groundwater-related risks at subsurface excavation sites. Eng. Geol. 125, 35–44. http://dx.doi.org/10.1016/j.enggeo.2011.10.015.

Kunstmann, H., Kastens, M., 2006. Determination of stochastic well head protection zones by direct propagation of uncertainties of particle tracks. J. Hydrol. 323 (1–4), 215–229. http://dx.doi.org/10.1016/j.jhydrol.2005.09.003.

Lee, S.-Y., Carle, S.F., Fogg, G.E., 2007. Geologic heterogeneity and a comparison of two geostatistical models: sequential Gaussian and transition probability-based geostatistical simulation. Adv. Water Resour. 30, 1914–1932.

Mariethoz, G., Renard, Ph., Cornaton, F., Jaquet, O., 2009. Truncated plurigaussian simulations to characterize aquifer heterogeneity. Ground Water. 47, 13–24.

McDonald, M.G., Harbaugh, A.W., 1988. A modular three-dimensional finite-difference ground-water flow model. Techniques of Water-Resources Investigations of the United States Geological Survey, Book 6 (Chapter A1).

Nolan, J.P., 2001. Maximum likelihood estimation of stable parameters. In: Barndorff-Nielsen, O.E., Mikosch, T., Resnick, S.I. (Eds.), Levy Processes: Theory and Applications. Birkhäuser, Boston, pp. 379–400.

Nowak, W., Schwede, R.L., Cirpka, O.A., Neuweiler, I., 2008. Probability density functions of hydraulic head and velocity in three-dimensional heterogeneous porous media. Water Resour. Res. 44, W08452. http://dx.doi.org/10.1029/2007WR006383.

Osnes, H., 1995. Stochastic analysis of head spatial variability in bounded rectangular heterogeneous aquifers. Water Resour. Res. 31 (12), 2981–2990.

Riva, M., Guadagnini, A., 2009. Effects of evolving scales of heterogeneity on hydraulic head predictions under convergent flow conditions. Hydrogeol. J. 17, 817–825. http://dx.doi.org/10.1007/s10040-008-0396-9.

Riva, M., Guadagnini, L., Guadagnini, A., Ptak, T., Martac, E., 2006. Probabilistic study of well capture zones distribution at the Lauswiesen field site. J. Cont. Hydrol. 88, 92–118.

Riva, M., Guadagnini, A., Fernández-García, D., Sánchez-Vila, X., Ptak, T., 2008. Relative importance of geostatistical and transport models in describing heavily tailed breakthrough curves at the Lauswiesen site. J. Contam. Hydrol. 101, 1–13.

Riva, M., Guadagnini, L., Guadagnini, A., 2010. Effects of uncertainty of litho-facies, conductivity and porosity distributions on stochastic interpretations of a field-scale tracer test. Stoch. Env. Res. Risk. A 24, 955–970. http://dx.doi.org/10.1007/s00477-010-0399-7.

Rubin, Y., Dagan, G., 1988. Stochastic analysis of boundaries effects on head spatial variability in heterogeneous aquifers: 1. Constant head boundary. Water Resour. Res. 24 (10), 1689–1697.

Rubin, Y., Dagan, G., 1989. Stochastic analysis of boundaries effects on head spatial variability in heterogeneous aquifers: 2. Impervious boundary. Water Resour. Res. 25 (4), 707–712.

Samorodnitsky, G., Taqqu, M., 1994. Stable Non-Gaussian Random Processes. Chapman and Hall, New York.

Scheibe, T.D., Murray, C.J., 1998. Simulation of geologic patterns: a comparison of stochastic simulation techniques for groundwater transport modelling. In: Fraser, G.S., Davis, J.M. (Eds.), Special Publication of the SEPM (Society for Sedimentary Geology). Tulsa, OK, pp. 107–118.

Schwede, R.L., Cirpka, O.A., Nowak, W., Neuweiler, I., 2008. Impact of sampling volume on the probability density function of steady state concentration. Water Resour. Res. 44, 12. http://dx.doi.org/10.1029/2007WR006668.

Strebelle, S., 2002. Conditional simulation of complex geological structures using multiple point statistics. Math. Geosci. 34, 1–22.

Tartakovsky, D.M., 2013. Assessment and management of risk in subsurface hydrology: a review and perspective. Adv. Water Resour. 51, 247–260. http://dx.doi.org/10.1016/j.advwatres.2012.04.007.

Vassena, C., Rienzner, M., Ponzini, G., Giudici, M., Gandolfi, C., Durante, C., Agostani, D., 2012. Modeling water resources of a highly irrigated alluvial plain (Italy): calibrating soil and groundwater models. Hydrogeol. J. 20 (3), 449–467. http://dx.doi.org/10.1007/s10040-011-0822-2.

Winter, C.L., Tartakovsky, D.M., Guadagnini, A., 2003. Moment differential equations for flow in highly heterogeneous porous media. Surveys Geophys. 24 (1), 81–106.

Wu, J., Boucher, A., Zhang, T., 2008. SGeMS code for pattern simulation of continuous and categorical variables: FILTERSIM. Comput. Geosci. 34 (728), 1863–1876.

Xu, C., Dowd, P.A., Mardia, K.V., Fowell, R.J., 2006. A flexible true plurigaussian code for spatial facies simulations. Comput. Geosci. 32, 1629–1645.

Zarlenga, A., Fiori, A., Soffia, C., Jankovic, I., 2012. Flow velocity statistics for uniform flow through 3D anisotropic formations. Adv. Water Resour. 40, 37–45.

Zhang, T., Switzer, P., Journel, A.G., 2006. Filter-based classification of training image patterns for spatial simulation. Math. Geosci. 38, 63–80.